

# Spatial Resolution Improvement with Variable Field-of-View Continuously Moving Table MRI

H. H. Hu<sup>1</sup>, A. J. Madhuranthakam<sup>1</sup>, D. G. Kruger<sup>1</sup>, J. F. Glockner<sup>1</sup>, S. J. Riederer<sup>1</sup>

<sup>1</sup>Dept. of Radiology, Mayo Clinic College of Medicine, Rochester, Minnesota, United States

## Introduction

In peripheral 3D CE-MRA, lateral spatial resolution in coronally-acquired angiograms becomes critical as distal vessel diameters approach several millimeters or less. In continuously moving table (CMT) CE-MRA, spatial resolution is further dependent on the actively-sampled sub-FOV (FOV<sub>s</sub>), the repetition time TR, and the table velocity used. Methods to improve spatial resolution in CMT have been introduced, including a dual-velocity technique that slows the table to match the contrast bolus in the distal vessels such that more views are acquired [1], and parallel-imaging [2,3]. Alternatively, peripheral CE-MRA with discrete multi-station approaches offers the flexibility of tailoring parameters such as FOV, slice thickness, and the imaging matrix size to the vasculature of interest at every station [4,5]. On the contrary, in CMT the lateral and slice FOV have thus far been held constant for the entire longitudinal extent, with values typically determined by the widest portion of the peripheral vasculature. The purpose of this work is to implement a technique in which the lateral FOV<sub>s</sub> can be dynamically changed during table motion. The FOV<sub>s</sub> transition occurs at an operator-specified location along the longitudinal axis, and improvement in lateral spatial resolution is provided in the imaging region where the FOV<sub>s</sub> is reduced. The technique is demonstrated with phantom and volunteer peripheral CE-MRA results.

## Methods

The k-space implications of variable-FOV CMT have been previously described [6]. Fig.1 summarizes the effects on k-space sampling when the acquisition FOV<sub>s</sub> is dynamically switched during CMT. For illustration simplicity, the FOV<sub>s</sub> transition occurs after one complete view cycle and a 2D example using hybrid k-space (X-k<sub>Y</sub>-k<sub>Z</sub>) is shown. Constant table velocity and sequential view order are assumed. As discussed in Ref. 6, areas containing data solely from FOV<sub>s1</sub> (Region 1) and FOV<sub>s2</sub> (Region 3) can undergo standard Fourier transformation (FT). However, data along any line of fixed X in Region 2 has been acquired by two different  $\Delta k_Y$  sampling intervals with a specific sampling pattern for each X-location. Interpolation must be performed to restore a uniformly sampled k-space prior to FT.

**Phantom:** Contrast-filled tubing and a resolution bar phantom were assembled. Bars were oriented along the Y-axis to demonstrate improvement in left/right spatial resolution with variable-FOV CMT. A 3D spoiled GRE sequence was used: TR/TE = 6/1.8 ms, 256 (read)×128(phase)×16 (slice), FOV<sub>s</sub> = 18 cm, FOV<sub>s1</sub>/FOV<sub>s2</sub> = 32/20 cm, and 5.5 mm slices. The longitudinal FOV was approximately 120 cm and the FOV switch occurred after 54 cm of table travel.

**CE-MRA Volunteers:** Seven volunteers underwent IRB-approved peripheral CE-MRA exams with the variable-FOV CMT method. All studies were performed on a 1.5T GE Signa scanner. Coronal slices were acquired with a 3D spoiled GRE sequence and sequential view-order. Acquisition parameters were determined from localizers. FOV<sub>s1</sub> was typically used to image from the renal artery origins to the femoral arteries, while FOV<sub>s2</sub> was used to image the popliteal trifurcation to the pedal arteries. All other parameters remained constant during the exam, shown in Table 1 for two representative cases. 30 mL of Gd-contrast agent followed by equal saline was injected at 2.0 mL/s for each study. A pre-contrast mask of the extended anatomy was acquired. Table motion was fluoroscopically triggered upon contrast arrival in the abdominal aorta. Offline reconstruction yielded artifact-free images with good vessel enhancement and continuity in all cases.

## Results

Fig.2a shows raw FT reconstruction of variable-FOV CMT data from the phantom without k<sub>Y</sub>-space interpolation in Region 2. The dashed line marks the X-location where FOV<sub>s</sub> was switched from 32 to 20 cm. Note dual image artifacts of the contrast-filled tube (arrowheads). Fig.2b shows reconstruction after interpolation, with removal of signals from the larger 32 cm frame in Region 2. The distal FOV<sub>s2</sub> was chosen such that it closely circumscribes the resolution phantom. In Fig.2c, the enlargement of the resolution phantom shows improved left/right resolution compared to Fig.2d, the latter obtained from a separate CMT acquisition where FOV<sub>s</sub> was fixed at 32 cm throughout the extended X-axis.

Two volunteer mask-subtracted MIP images are shown in Fig.3. In both cases, note that FOV<sub>s1</sub> was used up to the iliac/femoral arteries, while vasculature below the dashed line was acquired with a smaller FOV<sub>s2</sub>. FOV<sub>s1</sub> was prescribed to adequately image the femoral branches, while FOV<sub>s2</sub> circumscribes the anterior tibial and pedal arteries. Lateral spatial resolution improvement is expected distally since the sampling matrix was kept constant throughout.

## Conclusion

The variable-FOV CMT allows dynamic changes in the lateral FOV to improve local lateral spatial resolution, and can easily be extended to additional view-orders, surface coils, and other CMT applications, such as whole-body screening. The technique has been successfully implemented *in vivo*.

## References

- [1] Kruger, et al. Proc. ISMRM 2004:233 (MRM article in press).  
 [2] Keupp, et al. Proc. ISMRM 2004:324.  
 [3] Hu, et al. Proc. ISMRM 2004:325.  
 [4] Maki, et al. JMRI 2001; 15:484-491.  
 [5] Leiner, et al. JMRI 2004; 20:417-425.  
 [6] Hu, et al. Proc. ISMRM 2003:1073.

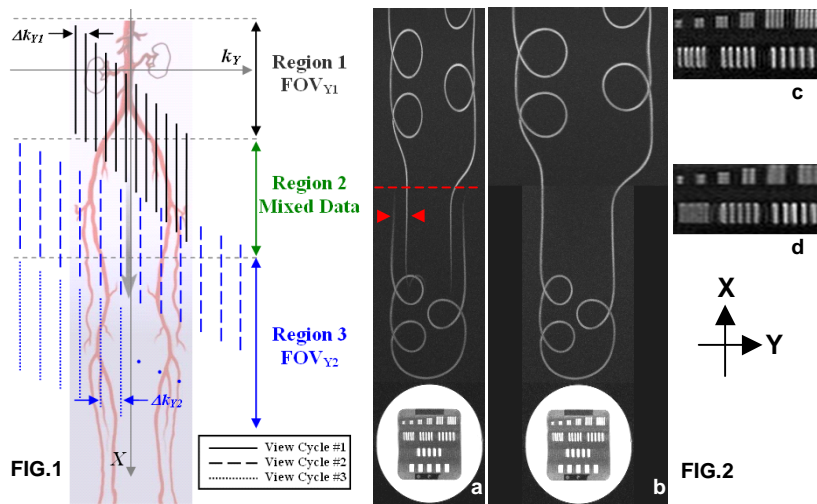


FIG.1

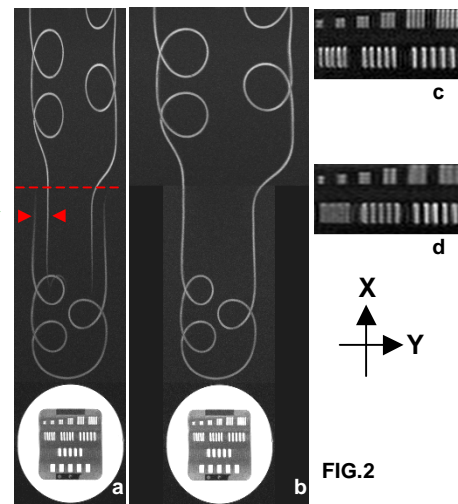


FIG.2

Table 1: Parameters for Volunteer Studies	Fig. 3a	Fig. 3b
FOV <sub>s</sub> (cm)	20	40
FOV <sub>s1</sub> (cm)	30	30
FOV <sub>s2</sub> (cm)	21	24
TR/TE (ms)	4.9/1.4	4.9/2.0
Matrix (read/phase/slice)	256/128/16	256/128/32
Slice thickness (mm)	7	3.2
Receiver	body	body

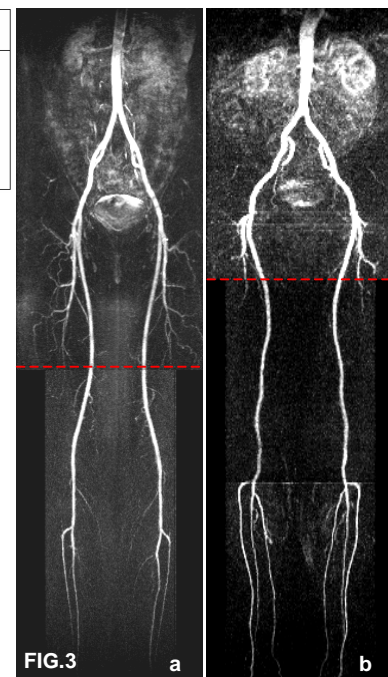


FIG.3